

CMS-LSTM: Context-Embedding and Multi-Scale Spatiotemporal-Expression LSTM for Video Prediction

Zenghao Chai¹, Chun Yuan^{1,3*}, Zhihui Lin^{1,2} and Yunpeng Bai¹

¹Shenzhen International Graduate School, Tsinghua University, Shenzhen, China

²Department of Computer Science and Technologies, Tsinghua University, Beijing, China

³Peng Cheng Laboratory, Shenzhen, China

zenghaochai@gmail.com, yuanc@sz.tsinghua.edu.cn, {lin-zh14,byp20}@mails.tsinghua.edu.cn

Abstract

Extracting variation and spatiotemporal features via limited frames remains as an unsolved and challenging problem in video prediction. Inherent uncertainty among consecutive frames exacerbates the difficulty in long-term prediction. To tackle the problem, we focus on capturing context correlations and multi-scale spatiotemporal flows, then propose CMS-LSTM by integrating two effective and lightweight blocks, namely Context-Embedding (CE) and Spatiotemporal-Expression (SE) block, into ConvLSTM backbone. CE block is designed for abundant context interactions, while SE block focuses on multi-scale spatiotemporal expression in hidden states. The newly introduced blocks also facilitate other spatiotemporal models (e.g., PredRNN, SA-ConvLSTM) to produce representative implicit features for video prediction. Qualitative and quantitative experiments demonstrate the effectiveness and flexibility of our proposed method. We use fewer parameters to reach markedly state-of-the-art results on Moving MNIST and TaxiBJ datasets in numbers of metrics. All source code is available at <https://github.com/czh-98/CMS-LSTM>.

1 Introduction

Spatiotemporal predictive learning has become a challenging but essential field in computer vision. Video prediction is one of the hotspots in spatiotemporal learning with board research prospects. It has benefited or could benefit plenty of applications, e.g., meteorological prediction [Shi *et al.*, 2015], traffic flows prediction [Xu *et al.*, 2018; Zhang *et al.*, 2017], and physical object movement [Lerer *et al.*, 2016]. The core task and challenge of video prediction are predicting future sequences based on limited observed frames.

Nevertheless, video sequences contain inherent complex semantic features, whereas the certainty of frames is exceptionally fuzzy. Therefore, it is crucial but hard to extract abundant implicit context features to overcome the uncertainty. It is usually necessary to take both target overlap, scale changes

into consideration, making the video prediction more challenging.

Recent years have seen significant progress in video prediction. Numerous researchers have carried out in-depth research in spatiotemporal predictive learning and proposed a series of RNN-based [Werbos, 1990; Hochreiter and Schmidhuber, 1997] models, from the original ConvLSTM [Shi *et al.*, 2015] used for precipitation nowcasting to the improved methods proposed based on ConvLSTM in recent years, such as PredRNN [Wang *et al.*, 2017], PredRNN++ [Wang *et al.*, 2018], MIM [Wang *et al.*, 2019b], E3D-LSTM [Wang *et al.*, 2019a], SA-ConvLSTM [Lin *et al.*, 2020]. These methods have achieved remarkable results in video prediction.

However, most of the previous work merely focuses on global spatiotemporal flows of given frames in hidden states, resulting in more extra parameters and ignorance of multi-scale variations between sequences. On the other hand, the input and context always perform independently in previous work. The relationship between the two is unidimensional. Namely, they did not pay enough attention to the interaction of context. With the increase of models' depth and complexity, correlations between the current input and upper context will decline as information flows among layers.

In this paper, to overcome deficiencies of the unidimensional relationship of context in previous work and pay more attention to multi-scale spatiotemporal flows, we propose Context-Embedding and Multi-Scale Spatiotemporal-Expression LSTM (CMS-LSTM), an extension structure of ConvLSTM. Specifically, 1) Context-Embedding (CE) block is designed to enhance the input and context interactions and correlations. 2) Multi-Scale Spatiotemporal-Expression (SE) block is designed based on the attention mechanism to capture abundant spatiotemporal flows in different scales. The main contributions are as follows:

- Two effective blocks are designed, namely Context-Embedding (CE) block and Spatiotemporal-Expression (SE) block. CE block can maintain consistency and extract further correlations between the current input and upper context. SE block can facilitate multi-scale dominant spatiotemporal flows' expression and weaken the negligible ones simultaneously.

- To the best of our knowledge, the proposed CMS-LSTM

*Contact Author

innovatively integrates context interaction enhancement and multi-scale spatiotemporal expression mechanism. It achieves state-of-the-art results on Moving MNIST and TaxiBJ datasets in numbers of metrics comparing with previous models.

- Numerous detailed qualitative and quantitative experiments have demonstrated the importance of context interactions and multi-scale spatiotemporal flows in video prediction. The proposed CE block and SE block have the portability to transplant in other models.

2 Related Work

RNN [Werbos, 1990] and its improved structure LSTM [Hochreiter and Schmidhuber, 1997] have been extensively used in spatiotemporal predictive learning in recent years. ConvLSTM [Shi *et al.*, 2015] based models are a crucial branch in video prediction. PredRNN [Wang *et al.*, 2017] and PredRNN++ [Wang *et al.*, 2018] improved predictive performance by introducing additional global memory cell and its reorganization. MIM [Wang *et al.*, 2019b] further updated memory cells into extra computation of non-stationary and stationary information for spatiotemporal expression. Moreover, E3D-LSTM [Wang *et al.*, 2019a] designed new 3D-CNN flows accompanied by a self-attention module as SA-ConvLSTM [Lin *et al.*, 2020] did for video prediction.

On the one hand, the context in previous spatiotemporal predictive work is independent, in ignorance of context correlation’s decrease as spatiotemporal information transmits among layers. e.g., SA-ConvLSTM [Lin *et al.*, 2020] designed an attention module for hidden states, regardless of previous input and upper context interactions. However, extraction of context correlations among state gates and enhancement of the relationship between these gating units are always a vital improving direction of LSTM. By extending the original LSTM, Mogrifier LSTM [Melis *et al.*, 2020] interacted current input with the upper context to maintain the correlation and extract implicit features by iterative calculation, demonstrating its effectiveness in multiple NLP tasks.

On the other hand, previous models above merely focus on global spatiotemporal features, regardless of the expression in multi-scales with different attention. However, Spatiotemporal flows are essential for inference in video prediction. Convolution Layer [Krizhevsky *et al.*, 2017] can effectively focus on local features but lacks expressing the importance of spatiotemporal flows. Initially proposed and applied in NLP [Gehring *et al.*, 2017], the self-attention mechanism [Vaswani *et al.*, 2017] has successfully extended to CV [Chu *et al.*, 2017; Xu and Saenko, 2016] related tasks and achieved impressive results. [Lin *et al.*, 2020] firstly applied the self-attention mechanism into video prediction, proposed as SA-ConvLSTM, and achieved state-of-the-art results. Nevertheless, self-attention fails to capture spatiotemporal expression in different scales, which is indispensable in video prediction. To overcome the inherent weakness of self-attention, the multi-scale attention mechanism, a method widely used in image detection [Zhao and Wu, 2019], image restoration [Mei *et al.*, 2020], and other fields, has shown great advantages in fine-grained feature extraction.

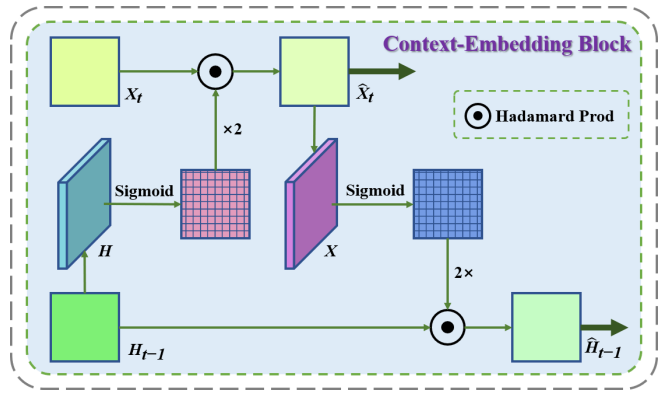


Figure 1: The pipeline of proposed CE block, where H_{t-1} , X_t are the previous state and current input, respectively. H and X are 5×5 convolution layers to extract features of H_t and \hat{X}_t , respectively. \hat{H}_{t-1} and \hat{X}_t are the output of CE block, representing the previous state and current input after context embedding, respectively.

3 Methods

3.1 CE Block

In previous RNN and LSTM based models, the input x_t and the previous state h_{t-1} are completely independently entering into LSTM layers. In other words, the two interact in LSTM in a unidimensional spatiotemporal state. Therefore, correlations between the current input and upper context tend to disappear as models become increasingly complex.

To explore the relationship between input and context and extract further correlational information between the two, inspired by the previous work [Melis *et al.*, 2020], we construct CE block to correlate the two states by iterative interaction, and the pipeline of CE block is illustrated in Figure 1.

Formally, context correlations are extracted by the interaction mode as Formula 1 in the proposed CE block.

$$\begin{aligned}\hat{X}_t &= 2 \times \sigma(W_H \star H_{t-1} + b_H) \circ X_t \\ \hat{H}_{t-1} &= 2 \times \sigma(W_X \star \hat{X}_t + b_X) \circ H_{t-1}\end{aligned}\quad (1)$$

In CE block, X_t and H_{t-1} are correlated by two convolution layers and Hadamard product. To describe the association of them with richer interactions, we use stacked CE blocks to extract abundant correlational information further. In addition, to minimize the extra parameters, multi-layer stacked CE blocks share the same convolution layers.

3.2 SE Block

In this section, we emphasize the insufficiency of previous work in multi-scale spatiotemporal flow extractions and construct SE block for maximizing extract multi-scale implicit spatiotemporal flows to overcome previous weakness.

Previous RNN-based approaches mostly concentrate on modeling global spatiotemporal features and flows, regardless of multi-scale neighbor features among sequences. However, pixel-level and object-level changes between adjacent frames tend to occur in specific regions. Namely, these regions contain more implicit spatiotemporal flows than single scale frames, showing the great necessity to model multi-scale spatiotemporal expression.

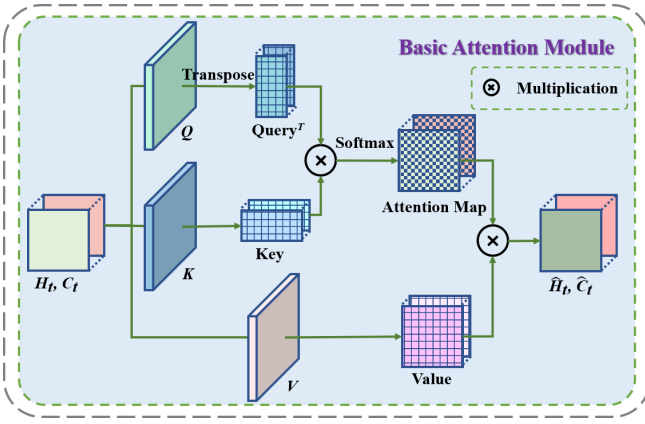


Figure 2: The architecture of basic attention module, where H_t and C_t are the output state and memory state of LSTM in a specific scale. K, Q, V are 1×1 convolution layers to obtain $Key, Query, Value$, respectively. \hat{H}_t and \hat{C}_t are the output of basic attention module.

The self-attention mechanism [Vaswani *et al.*, 2017] can effectively focus on important parts of the given feature map. We construct SE block based on self-attention mechanism, pipeline illustrated in Figure 2.

To reduce parameter consumption and improve efficiency as much as possible, we use a weight-shared attention module to share the weight of K, Q, V for H_t and C_t and calculate them in parallel.

In Figure 2, H_t and C_t constitute the input of basic attention module. $Key, Query$, and $Value$ are calculated through three 1×1 convolution layers K, Q, V separately. Then, Attention Map is obtained by $Softmax$ the multiplication of $Query^T$ and Key . The output is the multiplication of Attention Map and value.

$$\hat{H}_t, \hat{C}_t = Softmax(Query^T \times Key) \times Value \quad (2)$$

In LSTM, H_t and C_t contain spatiotemporal flows of given frames, while multi-scale neighbors in adjacent frames contain more implicit features than single-scale ones. In other words, multi-scale regions can extract pixel-level and object-level spatiotemporal flows among contexts and contain more potential tendencies.

Inspired by previous work [Zhao and Wu, 2019; Mei *et al.*, 2020; Chen and Shi, 2020], we construct SE block for implicit feature expression in multi-scale neighbors to extract spatiotemporal flows. The architecture of SE block is illustrated in Figure 3. In the SE block, the extraction of multi-scale spatiotemporal flows can be divided into two parts:

Part 1. Multi-Scale Spatiotemporal Features Expression The spatiotemporal states $H_t, C_t \in \mathbb{R}^{C \times H \times W}$ are stacked into $Z \in \mathbb{R}^{C \times H \times W \times 2}$. According to segmentation rules $R = R_1, \dots, R_n$, Z is divided into n multi-scale groups Z_1, \dots, Z_n (three groups in Figure 3), and each $Z_i, i \in [1, n]$ is stacked in C channel to compose z_1, \dots, z_n . Then the multi-scale implicit features $\hat{z}_1, \dots, \hat{z}_n$ are expressed by attention mechanism in Figure 2.

After that, the multi-scale implicit features are restored in H and W channels accompanied by concat operation in C

channel to composing \hat{Z} . Ultimately, feature maps A_H and A_C are calculated by 5×5 convolution layer taking $\hat{Z} \in \mathbb{R}^{n_C \times H \times W \times 2}$ as input and separated in the last channel.

Part 2. Spatiotemporal Implicit States Update A_H and A_C are stacked in C channel as the input of 5×5 convolution layer to obtain multi-scale Attention Map A . Updated implicit state \hat{Z}_H is obtained by summation of A and 5×5 convolution layer processed implicit state Z_H , and is split into 3 parts: i_t, g_t , and o_t , respectively. The memory state \hat{C}_t is further updated as follows:

$$\begin{aligned} i_t &= \sigma(W_{Ai} \star [A_H, A_C] + W_{hi} \star Z_H + b_i) \\ g_t &= \tanh(W_{Ag} \star [A_H, A_C] + W_{hg} \star Z_H + b_g) \\ \hat{C}_t &= (1 - i_t) \circ C_t + i_t \circ g_t \end{aligned} \quad (3)$$

Then, the output state \hat{H}_t is the dot product result between the output gate o_t and updated memory state \hat{C}_t , which can be formulated as follows:

$$\begin{aligned} o_t &= \sigma(W_{Ao} \star [A_H, A_C] + W_{ho} \star Z_H + b_o) \\ \hat{H}_t &= o_t \circ \hat{C}_t \end{aligned} \quad (4)$$

3.3 CMS-LSTM

As mentioned above, our goals are to maintain the spatiotemporal consistency and correlations among frames in LSTM layers, facilitate multi-scale dominant spatiotemporal flows' expression and weaken the negligible ones simultaneously.

Therefore, CMS-LSTM is constructed specially by taking both considerations of context interactions and multi-scale spatiotemporal flows. The architecture of proposed CMS-LSTM is illustrated in Figure 4.

Formally, the calculation process of CMS-LSTM can be expressed as follows:

$$\begin{aligned} \hat{X}_t, \hat{H}_{t-1} &= CE(\dots CE(X_t, H_{t-1})) \\ g_t &= \tanh(W_{xg} \star \hat{X}_t + W_{hg} \star \hat{H}_{t-1} + b_g) \\ i_t &= \sigma(W_{xi} \star \hat{X}_t + W_{hi} \star \hat{H}_{t-1} + b_i) \\ f_t &= \sigma(W_{xf} \star \hat{X}_t + W_{hf} \star \hat{H}_{t-1} + b_f) \\ C_t &= f_t \circ C_{t-1} + i_t \circ g_t \\ o_t &= \sigma(W_{xo} \star \hat{X}_t + W_{ho} \star \hat{H}_{t-1} + b_o) \\ H_t &= o_t \circ \tanh(C_t) \\ \hat{H}_t, \hat{C}_t &= SE(H_t, C_t) \end{aligned} \quad (5)$$

In Formula 5, CE and SE represent the CE and SE block mentioned in Section 3.1 and 3.2, respectively. \hat{X}_t and \hat{H}_{t-1} represent the output of 5-layer stacked CE blocks accompany by intensive context interactions.

Then, H_t and C_t are obtained through LSTM gate operations, which merely contains limited global spatiotemporal flows at present. We thus adopt 3-scale SE block mentioned in Section 3.2 to extract multi-scale features for further spatiotemporal flows among neighbors, to obtain the final output \hat{H}_t and \hat{C}_t of CMS-LSTM.

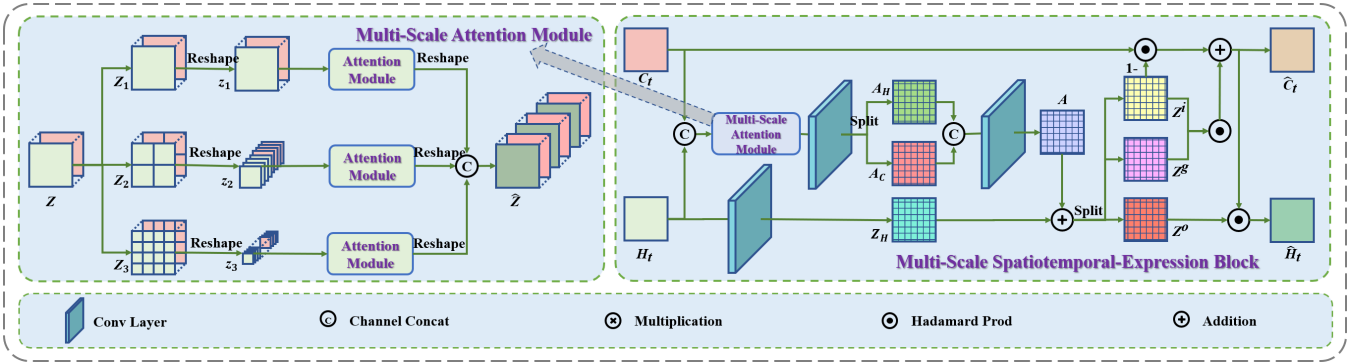


Figure 3: The pipeline of proposed SE block, where H_t and C_t represent the output of original ConvLSTM, and 5×5 convolution layers are used to extract features, \hat{H}_t and \hat{C}_t represent the output state and memory state after multi-scale spatiotemporal flows' extraction.

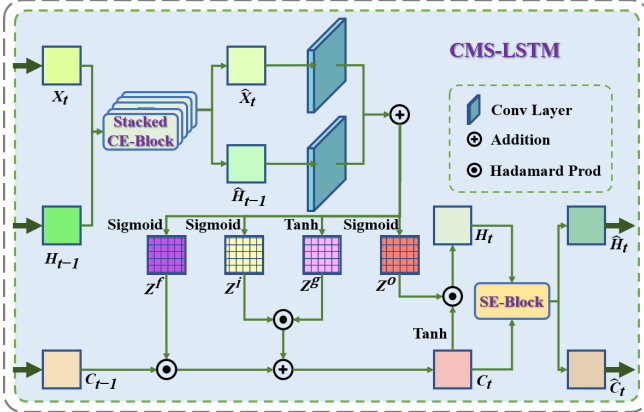


Figure 4: The architecture of CMS-LSTM. H_{t-1} and C_{t-1} represent the output state and memory state of $t-1$ time respectively, X_t represents the t time input, while \hat{H}_t and \hat{C}_t represent the output of CMS-LSTM, namely the output state and memory state of t time.

4 Experiments

4.1 Implementation Details

Pytorch [Paszke *et al.*, 2019] version of the proposed model is implemented. We use an RTX 2080Ti to train and test. For fair comparisons, the proposed model has the same architecture and similar computation load compared with previous work ([Wang *et al.*, 2017] etc.). We use the same 4-layer LSTM architecture with 64 hidden states. Setting mini-batch to 8 and initial learning rate to 0.001, scheduled sampling [Bengio *et al.*, 2015] and layer normalization [Ba *et al.*, 2016] are simultaneously adopted during training. We use L_2 loss for Moving MNIST and $L_1 + L_2$ loss for TaxiBJ with AdamW [Loshchilov and Hutter, 2017] optimizer to train the model.

4.2 Datasets

Moving MNIST

Moving MNIST [Srivastava *et al.*, 2015] is a commonly used dataset in video prediction, depicting 2 digits' movement with constant velocity. Each data contains $64 \times 64 \times 1$ consecutive frames with 10 for input and 10 for prediction, 10,000

randomly generate sequences for training and 10,000 fixed sequences for testing.

TaxiBJ

TaxiBJ [Xu *et al.*, 2018] is a traffic flow dataset collected from chaotic real-world environment, containing consecutive traffic flow images collected by GPS monitors of taxicabs in Beijing. Each frame in the dataset is a $32 \times 32 \times 2$ grid image, while each channel represents the traffic flow entering and leaving in same district. Following previous work, we generate 19,560 sequences for training and 1,344 sequences for testing, with 4 known frames to predict the next 4 frames.

4.3 Comparisons with SOTA Methods

We compare the proposed model with previous SOTA methods having the same architecture on Moving MNIST and TaxiBJ datasets quantitatively and randomly select the prediction results for qualitative comparisons to demonstrate our method's advantages and effectiveness. Other SOTA methods with different architectures and experiment settings are also quantitatively compared.

Results on Moving MNIST

We set 80,000 iterations consistent with previous work ([Wang *et al.*, 2017] etc.) and 400,000 iterations for better performance. Quantitative and qualitative comparisons are shown in Table 1 and Figure 5, respectively. Peak signal-to-noise ratio (PSNR), structural similarity (SSIM), mean square error (MSE) and mean absolute error (MAE) are used for quantitative comparisons. The performance improves as the SSIM and PSNR increase and the MSE and MAE decrease.

Results in Table 1 demonstrate the superiority of our method on Moving MNIST dataset in all above metrics, improving 14.5% and 3.9% on PSNR and SSIM, and reducing 41.7% and 33.4% on MSE and MAE respectively compared with previous SOTA methods having the same architecture.

Results in Figure 5 show that CMS-LSTM has better capability to capture variations over digits, especially deals with the trajectory of overlap digits and maintains the clarity over time. In contrast, predicted frames of other methods appear blurry in the digits and fail to deal with overlap digits.

More specifically, we give each metric's time-varying curves above on different models in Moving MNIST dataset

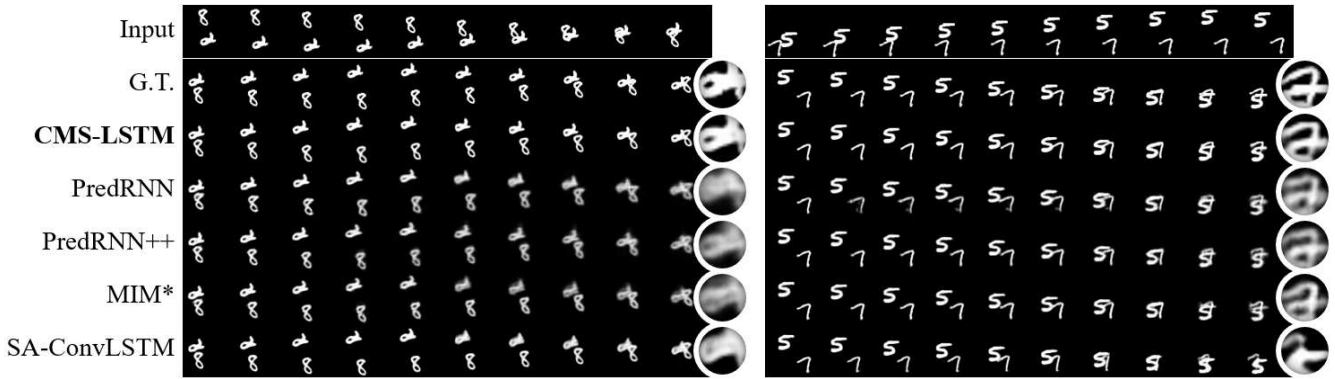


Figure 5: Qualitative comparisons of previous SOTA models on Moving MNIST test set at 80,000 iterations. The output frames are shown at one-frame intervals. We magnify the local of prediction results for additional detailed comparison at the last frame.

Table 1: Quantitative comparisons of previous SOTA models on Moving MNIST test set. All models predict 10 frames by observing 10 previous frames. We also try 400,000 iterations for higher performance.

Models	#Params	PSNR \uparrow	Δ	SSIM \uparrow	Δ	MSE \downarrow	Δ	MAE \downarrow	Δ
FC-LSTM [Srivastava <i>et al.</i> , 2015]	-	-	-	0.690	-	118.3	-	209.4	-
DDPAE [Hsieh <i>et al.</i> , 2018]	-	21.170	+1.567	0.922	+0.232	38.9	-79.4	90.7	-118.7
CrevNet+ConvLSTM [Yu <i>et al.</i> , 2020]	-	-	-	0.928	+0.238	38.5	-79.8	-	-
PhyDNet [Guen and Thome, 2020]	-	23.120	+3.517	0.947	+0.257	24.4	-93.9	70.3	-139.1
PDE-Driven [Donà <i>et al.</i> , 2021]	-	21.760	+2.157	0.909	+0.219	-	-	-	-
PredRNN [Wang <i>et al.</i> , 2017]	13.799 M	19.603	-	0.867	+0.177	56.8	-61.5	126.1	-83.3
PredRNN++ [Wang <i>et al.</i> , 2018]	13.237 M	20.239	+0.636	0.898	+0.208	46.5	-71.8	106.8	-102.6
MIM* [Wang <i>et al.</i> , 2019b]	27.971 M	20.678	+1.075	0.910	+0.220	44.2	-74.1	101.1	-108.3
E3D-LSTM [Wang <i>et al.</i> , 2019a]	38.696 M	20.590	+0.987	0.910	+0.220	41.7	-76.6	87.2	-122.2
SA-ConvLSTM [Lin <i>et al.</i> , 2020]	10.471 M	20.500	+0.897	0.913	+0.223	43.9	-74.4	94.7	-114.7
CMS-LSTM (80,000 iterations)	7.968 M	21.955	+2.352	0.931	+0.241	33.6	-84.7	73.1	-136.3
CMS-LSTM (400,000 iterations)	7.968 M	23.682	+4.079	0.949	+0.259	24.3	-94.0	58.1	-151.3

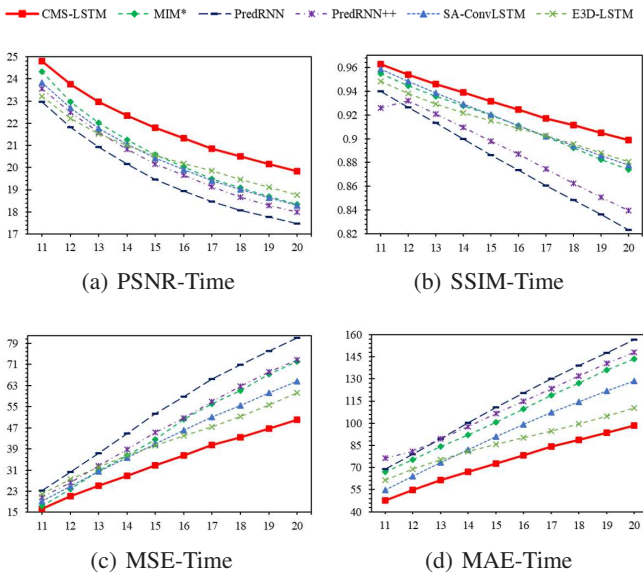


Figure 6: Frame-wise comparisons of the next 10 generated Moving MNIST frames at 80,000 iterations. The slower trend indicates better performance. The proposed CMS-LSTM is the most high-performing method overall timestamps in the forecasting horizon.

with 80,000 iterations, as shown in Figure 6.

Results in Figure 6 not only show that our method outperforms all the above methods in frame-wise prediction over these metrics but also represent the stability of our method in long-term prediction task. CMS-LSTM shows the best results and slowest performance decay in the forecasting horizon.

Results on TaxiBJ

We train the proposed model for 80,000 iterations for fair comparisons with previous methods ([Wang *et al.*, 2017] etc.). Quantitative and qualitative comparisons are shown in Table 2 and Figure 7, respectively.

As shown in Table 2, we adopt the frame-wise MSE as the metric. Smaller MSE indicates better performance. Compared with previous work, our method has the best performance and stability in traffic flow prediction, achieving over 41.5% average MSE reduction compared with previous SOTA models (SA-ConvLSTM).

The visualized comparisons with previous methods in Figure 7 include both the predicted frames and their absolute difference between ground truth. The brighter brightness represents higher absolute errors, whereas the proposed method shows the darkest brightness compared with other methods, further indicating the superiority of our method in dealing with uncertainty sequences.

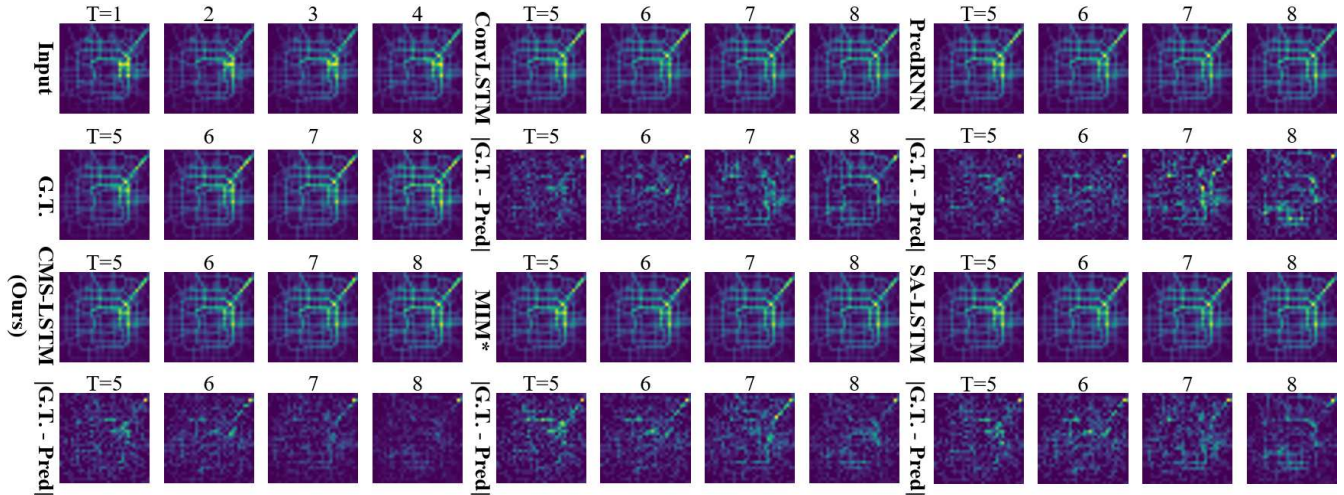


Figure 7: Qualitative comparisons of previous SOTA models on TaxiBJ test set. All models output the next 4 frames, accompanied by absolute difference with ground truth. Brighter brightness represents higher absolute errors.

Table 2: Frame-wise MSE comparisons of previous SOTA models on TaxiBJ test set. All models predict the next 4 frames (traffic conditions for the next 2 hours) via 4 historical traffic flow images.

Models	Frame1 ↓	Frame2 ↓	Frame3 ↓	Frame4 ↓	Average ↓	Δ
ST-ResNet [Zhang <i>et al.</i> , 2017]	0.460	0.571	0.670	0.762	0.618	-
VPN [Kalchbrenner <i>et al.</i> , 2017]	0.427	0.548	0.645	0.721	0.585	-0.033
FRNN [Oliu <i>et al.</i> , 2018]	0.331	0.416	0.518	0.619	0.471	-0.147
PhyDNet [Guen and Thome, 2020]	-	-	-	-	0.419	-0.199
PDE-Driven [Donà <i>et al.</i> , 2021]	-	-	-	-	0.398	-0.220
PredRNN [Wang <i>et al.</i> , 2017]	0.318	0.427	0.516	0.595	0.464	-0.154
PredRNN++ [Wang <i>et al.</i> , 2018]	0.319	0.399	0.500	0.573	0.448	-0.170
MIM* [Wang <i>et al.</i> , 2019b]	0.309	0.390	0.475	0.542	0.429	-0.189
SA-ConvLSTM [Lin <i>et al.</i> , 2020]	0.269	0.356	0.426	0.507	0.390	-0.228
CMS-LSTM	0.162	0.203	0.254	0.294	0.228	-0.390

5 Ablation Studies

To better illustrate the superiority of the proposed method, we conduct a series of ablation studies to verify the effectiveness of CE block and SE block, which focus on extractions of context interactions and multi-scale spatiotemporal flows. All experiments below set 80,000 iterations for training.

We verify the necessity of context interactions and multi-scale spatiotemporal flows by comparing CMS-LSTM removing CE block and SE block, respectively, and then using different scales to illustrate the necessity of the multi-scale spatiotemporal expression.

Besides, to testify the portability of CE block and SE block, we transplant the two blocks into previous work PredRNN and SA-ConvLSTM. Specifically, we compare PredRNN [Wang *et al.*, 2017] and SA-ConvLSTM [Lin *et al.*, 2020] with/without CE block and SE block in the same experiment settings using the same metrics as Section 4.3 for quantitative comparisons on Moving MNIST dataset, results shown in Table 3.

Results in Table 3 show the effectiveness of CE block and SE block. The entire CMS-LSTM achieves the best performance compared with the original ConvLSTM. Comparing models with and without CE block demonstrates the necessity of context interactions. Moreover, experiments in multi-scale further show the importance of spatiotemporal flow extrac-

Table 3: Ablation studies on Moving MNIST dataset. Models with and without CE block or SE block are tested sequentially in different backbones, as well as SE block with different scales in ConvLSTM.

Models	PSNR ↑	Δ	SSIM ↑	Δ	MSE ↓	Δ	MAE ↓	Δ
ConvLSTM	18.523	-	0.877	-	70.4	-	115.9	-
w CE, w/o SE	21.189	+2.666	0.918	+0.041	39.1	-31.3	82.8	-33.1
w CE, w 1-scale SE	21.708	+3.185	0.927	+0.050	35.1	-35.3	76.3	-39.6
w/o CE, w SE	21.712	+3.189	0.927	+0.050	34.8	-35.6	76.2	-39.7
w CE, w 2-scale SE	21.858	+3.335	0.929	+0.052	33.8	-36.6	74.3	-41.6
w CE, w SE	21.955	+3.432	0.931	+0.054	33.6	-36.8	73.1	-42.8
PredRNN	19.603	-	0.867	-	56.8	-	126.1	-
w CE, w/o SE	22.356	+2.753	0.924	+0.057	30.7	-26.1	82.7	-43.4
w/o CE, w SE	22.761	+3.158	0.931	+0.064	28.7	-28.1	76.9	-49.2
w CE, w SE	23.210	+3.607	0.935	+0.068	26.3	-30.5	74.2	-51.9
SA-ConvLSTM	20.500	-	0.913	-	43.9	-	94.7	-
w/o CE, w SE	20.970	+0.470	0.918	+0.005	39.8	-4.10	84.2	-10.5
w CE, w/o SE	22.591	+2.091	0.929	+0.016	27.3	-16.6	79.0	-15.7

tions in different scales.

Table 3 further verifies the portability of CE block and SE block. With the transplant of CE block and SE block, previous models' performances do get significantly improved, indicating the ability of our methods to be transplanted in other spatiotemporal predictive models.

6 Conclusions

This paper creatively proposes effective and lightweight modules focused on context interactions and multi-scale spatiotemporal expression named CE block and SE block, and then constructs CMS-LSTM, an extension architecture of ConvLSTM. Qualitative and quantitative experiments demonstrate the superiority of our method dealing with uncertainty and overlap in sequences, showing state-of-the-art performance in Moving MNIST and TaxiBJ datasets.

Ablation studies further verify the effectiveness and flexibility of our method. The proposed CE block can maintain the spatiotemporal consistency among long sequences, and SE block facilitates multi-scale dominant spatiotemporal flows' expression and weaken the negligible ones simultaneously. They can transplant to other spatiotemporal predictive related models to improve the performance markedly.

References

- [Ba *et al.*, 2016] Jimmy Lei Ba, Jamie Ryan Kiros, and Geoffrey E Hinton. Layer normalization. *arXiv preprint arXiv:1607.06450*, 2016.
- [Bengio *et al.*, 2015] Samy Bengio, Oriol Vinyals, Navdeep Jaitly, et al. Scheduled sampling for sequence prediction with recurrent neural networks. pages 1171–1179, 2015.
- [Chen and Shi, 2020] Hao Chen and Zhenwei Shi. A spatial-temporal attention-based method and a new dataset for remote sensing image change detection. *Remote. Sens.*, (10):1662, 2020.
- [Chu *et al.*, 2017] Xiao Chu, Wei Yang, Wanli Ouyang, et al. Multi-context attention for human pose estimation. In *CVPR 2017*, pages 5669–5678, 2017.
- [Donà *et al.*, 2021] Jérémie Donà, Jean-Yves Franceschi, sylvain lamprier, et al. Pde-driven spatiotemporal disentanglement. In *ICLR 2021*, 2021.
- [Gehring *et al.*, 2017] Jonas Gehring, Michael Auli, David Grangier, et al. Convolutional sequence to sequence learning. In *ICML 2017*, pages 1243–1252, 2017.
- [Guen and Thome, 2020] Vincent Le Guen and Nicolas Thome. Disentangling physical dynamics from unknown factors for unsupervised video prediction. In *CVPR 2020*, pages 11471–11481, 2020.
- [Hochreiter and Schmidhuber, 1997] Sepp Hochreiter and Jürgen Schmidhuber. Long short-term memory. *Neural computation*, (8):1735–1780, 1997.
- [Hsieh *et al.*, 2018] Jun-Ting Hsieh, Bingbin Liu, De-An Huang, et al. Learning to decompose and disentangle representations for video prediction. In *NeurIPS 2018*, pages 515–524, 2018.
- [Kalchbrenner *et al.*, 2017] Nal Kalchbrenner, Aäron van den Oord, Karen Simonyan, et al. Video pixel networks. In *ICML 2017*, pages 1771–1779, 2017.
- [Krizhevsky *et al.*, 2017] Alex Krizhevsky, Ilya Sutskever, and Geoffrey E Hinton. Imagenet classification with deep convolutional neural networks. *Communications of the ACM*, (6):84–90, 2017.
- [Lerer *et al.*, 2016] Adam Lerer, Sam Gross, and Rob Fergus. Learning physical intuition of block towers by example. pages 430–438, 2016.
- [Lin *et al.*, 2020] Zhihui Lin, Maomao Li, Zhuobin Zheng, et al. Self-attention convlstm for spatiotemporal prediction. In *AAAI 2020*, pages 11531–11538, 2020.
- [Loshchilov and Hutter, 2017] Ilya Loshchilov and Frank Hutter. Fixing weight decay regularization in adam. *CoRR*, 2017.
- [Mei *et al.*, 2020] Yiqun Mei, Yuchen Fan, Yulun Zhang, et al. Pyramid attention networks for image restoration. *arXiv preprint arXiv:2004.13824*, 2020.
- [Melis *et al.*, 2020] Gábor Melis, Tomás Kociský, and Phil Blunsom. Mogrifier LSTM. In *ICLR 2020*, 2020.
- [Oliu *et al.*, 2018] Marc Oliu, Javier Selva, and Sergio Escalera. Folded recurrent neural networks for future video prediction. In *ECCV 2018*, pages 745–761, 2018.
- [Paszke *et al.*, 2019] Adam Paszke, Sam Gross, Francisco Massa, et al. Pytorch: An imperative style, high-performance deep learning library. In *NeurIPS 2019*, pages 8024–8035, 2019.
- [Shi *et al.*, 2015] Xingjian Shi, Zhoung Chen, Hao Wang, et al. Convolutional lstm network: A machine learning approach for precipitation nowcasting. *Advances in neural information processing systems*, pages 802–810, 2015.
- [Srivastava *et al.*, 2015] Nitish Srivastava, Elman Mansimov, and Ruslan Salakhutdinov. Unsupervised learning of video representations using lstms. In *ICML 2015*, pages 843–852, 2015.
- [Vaswani *et al.*, 2017] Ashish Vaswani, Noam Shazeer, Niki Parmar, et al. Attention is all you need. In *NeurIPS 2017*, pages 5998–6008, 2017.
- [Wang *et al.*, 2017] Yunbo Wang, Mingsheng Long, Jianmin Wang, et al. Predrnn: Recurrent neural networks for predictive learning using spatiotemporal lstms. In *NeurIPS 2017*, pages 879–888, 2017.
- [Wang *et al.*, 2018] Yunbo Wang, Zhifeng Gao, Mingsheng Long, et al. Predrnn+: Towards A resolution of the deep-in-time dilemma in spatiotemporal predictive learning. pages 5110–5119, 2018.
- [Wang *et al.*, 2019a] Yunbo Wang, Lu Jiang, Ming-Hsuan Yang, et al. Eidetic 3d LSTM: A model for video prediction and beyond. In *ICLR 2019*, 2019.
- [Wang *et al.*, 2019b] Yunbo Wang, Jianjin Zhang, Hongyu Zhu, et al. Memory in memory: A predictive neural network for learning higher-order non-stationarity from spatiotemporal dynamics. In *CVPR 2019*, pages 9154–9162, 2019.
- [Werbos, 1990] Paul J Werbos. Backpropagation through time: what it does and how to do it. *Proceedings of the IEEE*, (10):1550–1560, 1990.
- [Xu and Saenko, 2016] Huijuan Xu and Kate Saenko. Ask, attend and answer: Exploring question-guided spatial attention for visual question answering. In *ECCV 2016*, pages 451–466, 2016.
- [Xu *et al.*, 2018] Ziru Xu, Yunbo Wang, Mingsheng Long, et al. Predcnn: Predictive learning with cascade convolutions. In *IJCAI 2018*, pages 2940–2947, 2018.
- [Yu *et al.*, 2020] Wei Yu, Yichao Lu, Steve Easterbrook, et al. Efficient and information-preserving future frame prediction and beyond. In *ICLR 2020*, 2020.
- [Zhang *et al.*, 2017] Junbo Zhang, Yu Zheng, and Dekang Qi. Deep spatio-temporal residual networks for citywide crowd flows prediction. In *AAAI 2017*, pages 1655–1661, 2017.
- [Zhao and Wu, 2019] Ting Zhao and Xiangqian Wu. Pyramid feature attention network for saliency detection. In *CVPR 2019*, pages 3085–3094, 2019.